J Solid State Electrochem (2008) 12:143–148
DOI 10.1007/s10008-007-0372-7

ORIGINAL PAPER

Microwave-assisted combustion synthesis of nanocrystalline $La_2Mo_2O_9$ oxide-ion conductor and its characterization

T. Saradha · S. Muzhumathi · A. Subramania

Received: 16 February 2007 / Revised: 13 April 2007 / Accepted: 4 June 2007 / Published online: 7 July 2007

Abstract Nanocrystalline $La_2Mo_2O_9$ oxide-ion conductor has been successfully synthesized by microwave-assisted combustion method within a very short time duration using aspartic acid as the newer fuel in a domestic microwave oven. The synthesized nanocrystalline powder showed good sinterability and reached more than 97% of theoretical density even at low temperature of 800 °C for 5 h. The sintered $La_2Mo_2O_9$ sample exhibited a conductivity of 0.159 S/cm in air at 750 °C.

Keywords $La_2Mo_2O_9$ · Oxide-ion conductor · Microwave-assisted combustion method · Aspartic acid · Ionic conductivity

Introduction

Recently, $La_2Mo_2O_9$-based oxide-ion conductors have attracted special attention, owing to their relatively high ionic conductivity at low temperatures (400–800 °C) under a wide oxygen partial pressure ranging from 0.21 to 10^{-17} atm [1–4]. Pure $La_2Mo_2O_9$ undergoes a phase transition from a slightly monoclinic low temperature α-form to a cubic high temperature β-form at about 580 °C [1, 2]. At this transition temperature, the conductivity of $La_2Mo_2O_9$ is abruptly increased by almost two orders of magnitude and reaching a value that is higher than yttria-stabilized zirconia (YSZ), the most widely used solid electrolyte for oxygen conduction.

$La_2Mo_2O_9$ is usually prepared by a conventional solid-state reaction method [1–5], but this method is not suitable to obtain dense ceramic samples because the ceramic grains grow excessively during the synthesis process. The grain growth decreases the sinterability and therefore, it is very difficult to obtain dense ceramic samples. After that, high dense $La_2Mo_2O_9$ have also been prepared by solid state reaction method, using ball milling to reduce the ceramic grain size; however, impurities of zirconia were detected [6, 7]. These impurities are usually located in the grain boundary after sintering and they considerably increase the grain boundary resistance. This grain boundary effect can lead to an overall reduction of the oxide-ion conductivity of the material. Therefore, high purity and high density are two key factors to obtain $La_2Mo_2O_9$-based oxide-ion conductors with excellent performance.

Nanocrystalline powders provide faster densification kinetics, lower sintering temperatures, better mechanical properties of the electrolytes, and generally improve the electrical properties [8]. In this respect, we have successfully synthesized nanocrystalline $La_2Mo_2O_9$ powder, very recently by a conventional combustion method using aspartic acid as the fuel. The synthesized nanocrystalline powder possessed high reactivity and good sinterability and produced dense samples even at 800 °C [9].

On the other hand, microwave-assisted synthesis of materials has also become more popular in recent years, which enables to synthesize a high pure nanocrystalline powder at shorter time duration [10–12]. In the microwave field, because the microwave energy is absorbed directly by the bulk of the heated object rather than being conducted from the outside, uniform and rapid heating can be

T. Saradha · A. Subramania (✉)
Advanced Materials Research Laboratory,
Department of Industrial Chemistry, Alagappa University,
Karaikudi 630 003, India
e-mail: a_subramania@yahoo.co.in

S. Muzhumathi
Fuel Cell Division, Central Electrochemical Research Institute,
Karaikudi 630 006, India

achieved within a short time and at a temperature lower than that normally required. Therefore, energy consumption, processing time, and cost are reduced significantly. Hence, in the present investigation, an attempt has been made for the first time, to synthesize nanocrystalline $La_2Mo_2O_9$ powder from lanthanum nitrate, ammonium heptamolybdate, and aspartic acid as the newer combustion fuel by microwave-assisted combustion method. Aspartic acid is an amino acid; it is nontoxic and easily undergoes thermal polymerization to form a long chain linkage of aspartic acid (polyaspartic acid) [13]. This polyaspartic acid can act as an excellent fuel as well as a good dispersing agent in combustion process [9]. The La and Mo ions are trapped homogeneously throughout the polyaspartate matrix and effectively control the particle size to get the nanosized particles and keep the nanoparticles free from agglomeration during the combustion process. The synthesized product was characterized by XRD, TEM, and DSC analysis. In addition, sinterability, ionic conductivity, and ionic transport number were also studied.

Experimental

The nanocrystalline $La_2Mo_2O_9$ powder was synthesized by microwave-assisted combustion method using a domestic microwave oven operating at a frequency of 2.45 GHz with the maximum output power of 900 W. The flow chart procedure for the synthesis of $La_2Mo_2O_9$ is shown in Fig. 1. In this method, stoichiometric amounts of lanthanum nitrate ($La(NO_3)_3$), ammonium heptamolybdate ($(NH_4)_6$. Mo_7O_{24}) and aspartic acid were taken and made into a homogeneous solution using distilled water, the pH of the resulting solution is ~3. According to a concept developed in propellant chemistry [14], the required amount of aspartic acid was 0.4 M. The above homogeneous solution was taken in a glass beaker and kept in a microwave for 10 min irradiation to get a foam like metal-organic precursor. The foam-like powder was collected in the ceramic crucible and then exposed for different irradiation times at about 15 to 60 min to optimize the required irradiation time to get the final product.

The structural properties of the synthesized material in different microwave irradiation times were evaluated using X-ray diffraction studies (Model: Philips X'Pert MPD®). The diffraction patterns were recorded using Cu-Kα radiation at room temperature in the range of $10° \leq 2\theta \leq 70°$. The step size and scan rate were set at 0.1 and 0.02°, respectively. The chemical composition of the final compound was determined by inductively coupled plasma (ICP) emission spectroscopy, which confirmed the expected stoichiometry.

The particle size and morphology of the synthesized $La_2Mo_2O_9$ powder was observed by JEOL transmission electron microscopy (Model: 1200 EX). The phase transition was studied by differential scanning calorimetry (Model: Perkin-Elmer diamond) with a heating rate of 5 °C/min in air.

The synthesized nanocrystalline $La_2Mo_2O_9$ powder was pressed at 150 MPa into pellets with 10 mm diameter and 1.5-2 mm thickness using a die. The green density of

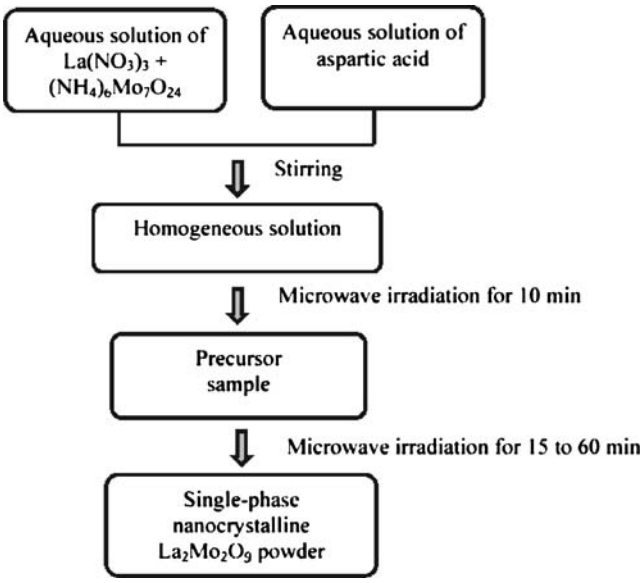

Fig. 1 Flow chart for synthesis of nanocrystalline $La_2Mo_2O_9$ powder by microwave-assisted combustion method

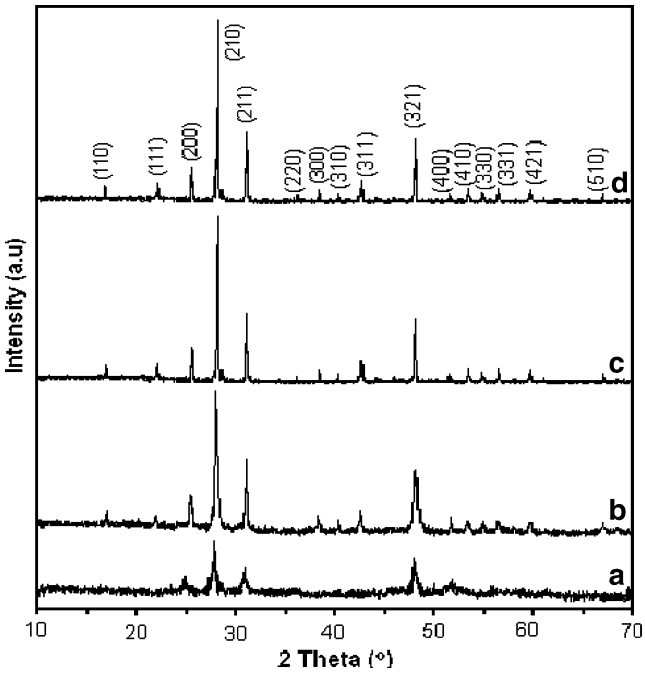

Fig. 2 X-ray diffraction patterns of $La_2Mo_2O_9$ prepared with different microwave irradiation times: **a** 15, **b** 30, **c** 45, and **d** 60 min

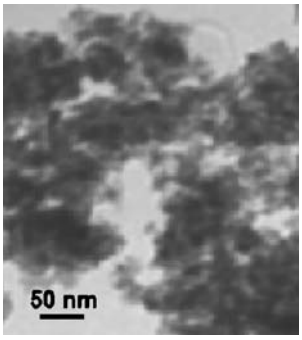

Fig. 3 TEM micrograph of the $La_2Mo_2O_9$ powder synthesized by microwave irradiation time for 45 min

pellets is ~62% of theoretical density. Nonisothermal sintering behavior of the green pellet was measured on a dilatometer (Model: Netzsch, DIL 402C) from room temperature to 900 °C at a heating rate of 5 °C/min and a cooling rate of 5 °C/min. Isothermal sintering was performed for the green pellet using a heating rate of 5 °C/min and a holding time of 5 h at various temperatures (600–900 °C). The density of the sintered pellet was also determined by the Archimedes' method using distilled water as the immersion medium. The microstructure of the sintered pellet was monitored by JEOL scanning electron microscopy (Model: JSM-840A).

The AC impedance spectra was collected over the frequency range of 0.1 Hz to 1 MHz, in the temperature range of 300–800 °C, using a Solartron-1260 impedance analyzer. The measurement procedure was described in detail elsewhere [9]. The oxygen-ion transference number was determined by the modified electromotive force (EMF) and faradaic efficiency (FE) methods, taking electrode polarization into account [15, 16]. The FE measurement was carried out under zero oxygen chemical potential gradient in air at 600–800 °C. The steady-state current density through the sample in the course of FE measurement was varied in the range of 0.01–20 mA/cm^2. The measurement of average transference number by the modified EMF technique was performed at 600–800 °C under the oxygen partial pressure gradients of 1.0/0.21 atm.

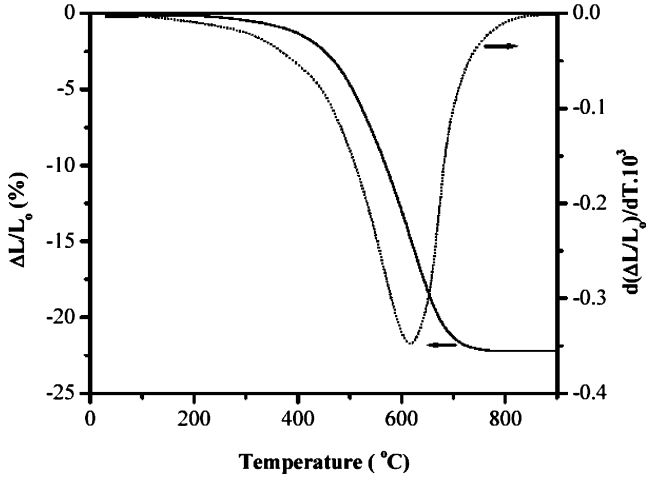

Fig. 5 Nonisothermal sintering behavior of $La_2Mo_2O_9$ pellet determined via dilatometer at a constant heating rate of 5 °C/min

Results and discussion

Figure 2 shows the X-ray diffraction patterns of $La_2Mo_2O_9$ powder synthesized at different microwave irradiation times. After irradiation at 15 min, significant peaks which represent $La_2Mo_2O_9$ begin to appear. The peaks became sharper with increasing the irradiation time to 45 min, indicating that a $La_2Mo_2O_9$ powder with better crystallinity was obtained. With further increasing the irradiation time to 60 min there is no improvement in

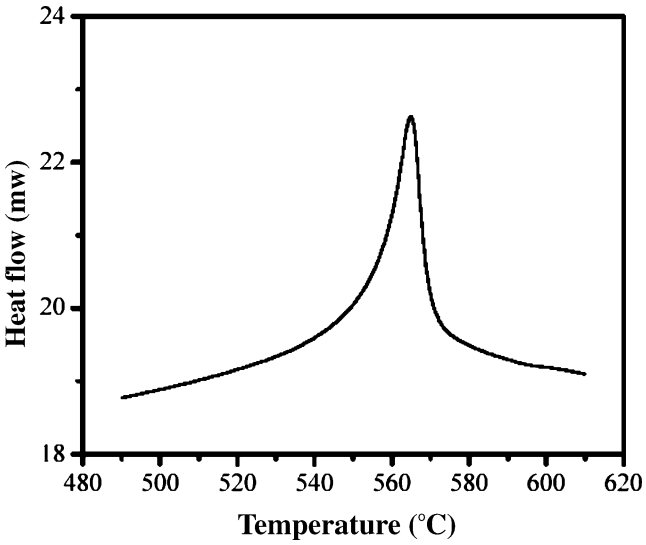

Fig. 4 DSC curve of nanocrystalline $La_2Mo_2O_9$ powder obtained from microwave irradiation time for 45 min

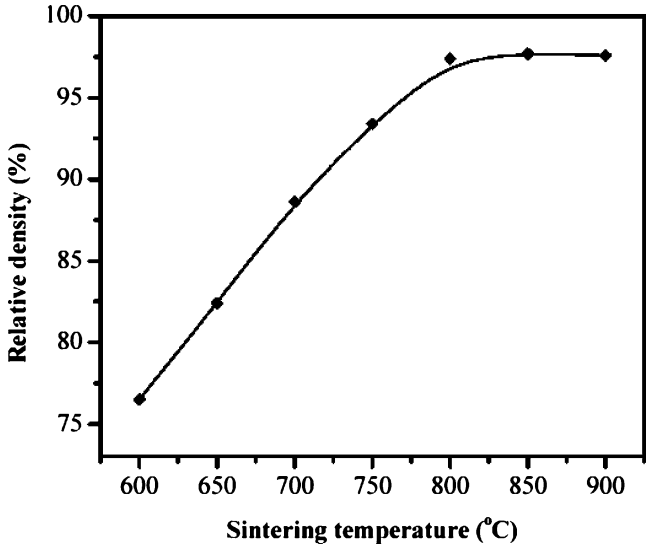

Fig. 6 Relative density of $La_2Mo_2O_9$ pellets isothermally sintered at 600–900 °C for 5 h

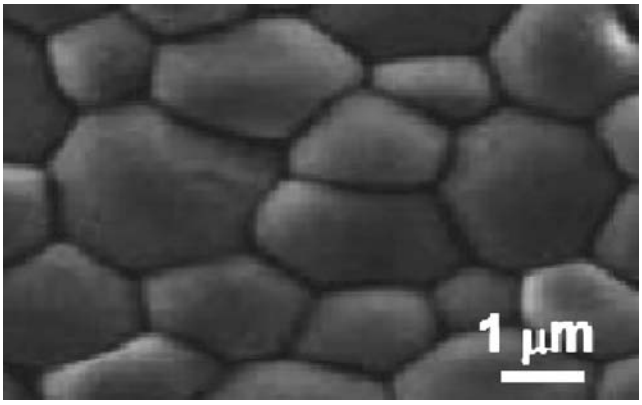

Fig. 7 SEM micrograph of $La_2Mo_2O_9$ pellet sintered at 800 °C for 5 h

the intensity of observed peaks. It revealed that the optimum irradiation time to the formation of well-defined crystalline $La_2Mo_2O_9$ powder is 45 min. The lattice parameter calculated for the synthesized product obtained with 45 min irradiation time has lattice constant value a = 7.1540(5)Å, which is in good agreement with literature value [17, 18]. Chemical analysis of the synthesized material was determined by inductively coupled plasma (ICP) emission spectroscopy. The result is exactly the same as the designed value which is La:Mo=2:2, it is proved that the stoichiometric $La_2Mo_2O_9$ powder is easily synthesized by microwave-assisted combustion method.

The transmission electron microscope of the $La_2Mo_2O_9$ synthesized by microwave irradiation time of 45 min is shown in Fig. 3. It can be seen that the synthesized $La_2Mo_2O_9$ powder is nanocrystalline in nature and the average particle size is about ~30 nm. The DSC curve for the nanocrystalline $La_2Mo_2O_9$ powder is shown in Fig. 4. It shows sharp endothermic peak at around 565 °C. The endothermic peak observed at around 565 °C in the DSC curve for the nanocrystalline $La_2Mo_2O_9$ powder confirms the α→β phase transition of $La_2Mo_2O_9$ [1].

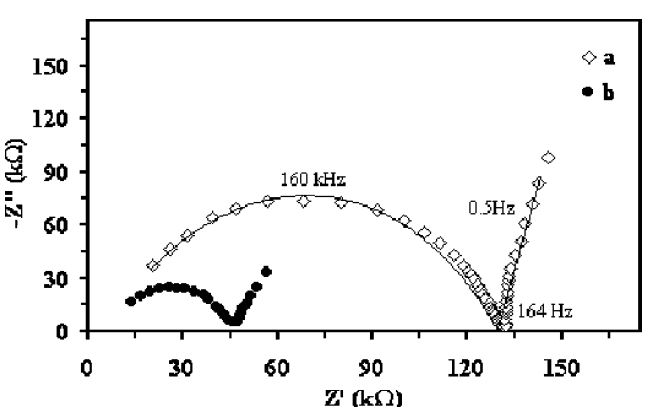

Fig. 8 Impedance spectra of sintered $La_2Mo_2O_9$ sample in air at **a** 350 and **b** 375 °C

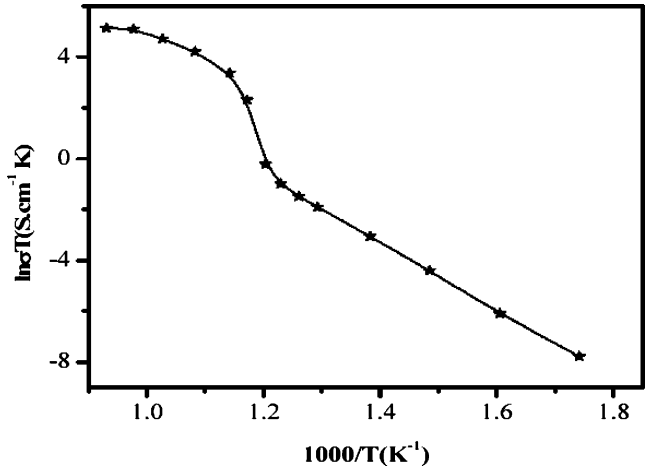

Fig. 9 Arrhenius plot of the overall conductivity of $La_2Mo_2O_9$ pellet sintered at 800 °C for 5 h

The nonisothermal behavior of the green compact determined via dilatometry under a constant heating rate of 5 °C is shown in Fig. 5. The compact has an initial green density of ~62% of theoretical density and shows quite good low temperature sintering activity. The shrinkage starts at ~360 °C and the maximum shrinkage rate is found at ~620 °C. The sintering process ends at about ~800 °C at which the total shrinkage of ~21.5% was recorded and the density is calculated to be greater than 97% of the theoretical density.

Relative density of the $La_2Mo_2O_9$ pellets isothermally sintered at 600–900 °C for 5 h are shown in Fig. 6. The relative density of this sample increases with increase in sintering temperature from 600 to 800 °C and becomes almost constant at higher temperature, which renders pellets up to ~98% dense. This sintering temperature is much lowered when compared with the sintering temperature of

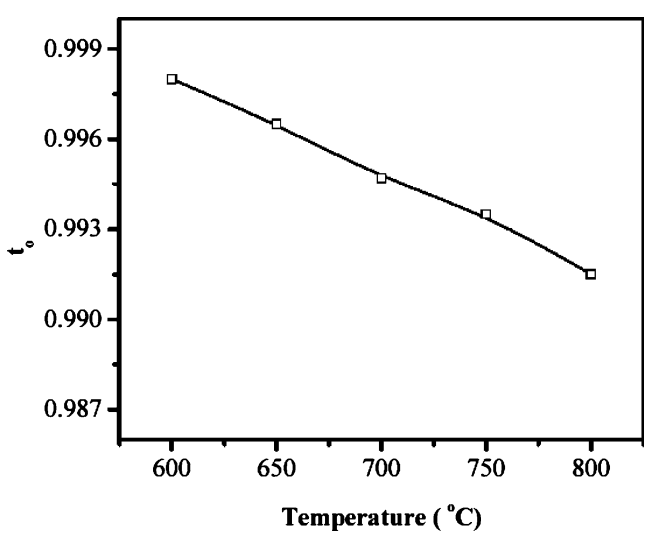

Fig. 10 Temperature dependence of the ionic transport number of $La_2Mo_2O_9$ under the oxygen partial pressure gradient of 1.0/0.21 atm

the product obtained by other reported methods [1–5]. This result indicates that the nanocrystalline nature of the synthesized powder is responsible for producing such a high sintered density at a low temperature. Moreover, the isothermal sintering behavior has good agreement with the nonisothermal sintering results. Figure 7 shows the scanning electron microscope of $La_2Mo_2O_9$ pellet sintered at 800 °C for 5 h. It shows the average grain size in the range of ~1–3 μm.

Figure 8 shows the impedance spectra of 800 °C sintered $La_2Mo_2O_9$ sample at two different temperatures of 350 and 375 °C. A high frequency semicircle is clearly visible in these impedance plots, indicating a distinct bulk (grain-interior) conductivity, but the medium-frequency associated with the grain boundary resistance is completely absent. The grain boundary effect is believed to arise from the presence of high resistance or blocking layer near grain boundaries, which in turn is believed to depend on the purity and microstructure of the material. Hence, the grain boundary effect can lead to an overall reduction of the oxide-ion conductivity of the material. The complete absence or a negligible grain boundary resistance or an overlapping of grain boundary arc has been reported earlier in nanocrystalline $La_2Mo_2O_9$ and CeO_2 materials [19–21]. George et al. [6] and Marrero-Lopez et al. [22] discussed the occurrence of grain boundary contributions in $La_2Mo_2O_9$, which is attributed to impurity segregation at the grain boundaries. In our previous work [9], complete absence of grain boundary resistance has been observed in nanocrystalline $La_2Mo_2O_9$ and established that the grain boundary effect has a detrimental effect on ionic conductivity and it could be eliminated completely, if impurities are not present in the ceramic. In the present work, we also have not seen any grain boundary effect; it was mainly attributed to the absence of impurity phase in the grain boundary and better connectivity between grains.

The Arrhenius plot for the overall conductivity of $La_2Mo_2O_9$ pellet sintered at 800 °C for 5 h is shown in Fig. 9. It shows clearly a first order phase transition at 565 °C with the increasing conductivity in the β-form and also this transition temperature is corroborating with our finding from DSC measurement. At 750 °C, it exhibits a conductivity of 0.159 S/cm. This conductivity value is somewhat higher compared to the same prepared by other reported methods [1, 19, 22]. The absence of a grain boundary arc in the impedance data along with a conductivity value of around 0.159 S/cm and a density more than 97% from our $La_2Mo_2O_9$ samples unequivocally establish the potential of this synthetic approach in developing impurity-free, phase pure, highly conducting, dense, and nanostructured lanthanum molybdate-based compounds for sensor and SOFC applications. Figure 10 represents the ionic transport number (t_o) of $La_2Mo_2O_9$ as a function of temperature. The estimated ionic transport number is slightly decreased with increasing temperature; however, it is higher than 0.99 in the measurement temperature range. This result demonstrates that the conductivity of $La_2Mo_2O_9$ is mainly ionic in nature.

Conclusions

A single-phase nanocrystalline $La_2Mo_2O_9$ oxide-ion conductor has been successfully synthesized by microwave-assisted combustion method using aspartic acid as the newer fuel, within a very short time of 45 min. The synthesized nanopowder was sintered to a density more than 97% of theoretical value even at relatively low temperature of 800 °C for 5 h. The sintered $La_2Mo_2O_9$ sample exhibited the conductivity of 0.159 S/cm in air at 750 °C and its ionic transport number was higher than 0.99 in the temperature range of 600–800 °C. Of special interest, in this study, is the absence of grain boundary contribution to overall resistance of the sintered ceramic, which was attributed to the cooperation of the excellent performance of high purity, high density, and phase homogeneity of the synthesized nanocrystalline powder, which can be expected to be applicable in the doped $La_2Mo_2O_9$ ceramic and other ceramic electrolytes.

Acknowledgement The authors thank Professor T. Vasudevan, Head, Department of Industrial Chemistry, for encouragement and support.

References

1. Lacorre P, Goutenoire F, Bohnke O, Retoux R, Laligant Y (2000) Nature 404:856
2. Goutenoire F, Isnard O, Retoux R, Lacorre P (2000) Chem Mater 12:2575
3. Georges S, Goutenoire F, Altorfer F, Sheptyakov D, Fauth F, Suard E, Lacorre P (2003) Solid State Ion 161:231
4. Yang J, Gu Z, Wen Z, Yan D (2005) Solid State Ion 176:523
5. Goutenoire F, Isnard O, Suard E, Bohnke O, Laligant Y, Retoux R, Lacorre P (2001) J Mater Chem 11:119
6. Georges S, Goutenoire F, Lacorre P, Steil MC (2005) J Eur Ceram Soc 25:3619
7. Georges S, Skinner S, Lacorre P, Steil MC (2004) Dalton Trans 19:3101
8. Rao CN, Gopalakrishnan S (1986) New directions in solid state chemistry. Cambridge University Press, Cambridge
9. Subramania A, Saradha T, Muzhumathi S (2007) J Alloys Compd, in press
10. Fu YP, Lin CH, Liu CW, Tay KW, Wen SB (2006) J Power Sources 159:38
11. Ryu JH, Yoon JW, Lim CS, Oh WC, Shim KB (2005) J Alloys Compd 390:245
12. Sundaram R, Raj ES, Nagaraja KS (2004) Sens Actuators B 99:350

13. Andini S, Benedetti E, Ferrara L, Paolillo L, Temussi PA (1975) Orig Life 6:147
14. Jain SR, Adiga KC, Pai Verneker VR (1981) Combust Flame 40:71
15. Kharton VV, Viskup AP, Figueiredo EM, Naumovich EN, Yaremchenko AA, Marques FMB (2001) Electrochim Acta 46:2879
16. Kharton VV, Marques FMB (2001) Solid State Ion 140:381
17. Tarancon A, Dezanneau G, Arbiol J, Peiro F, Morante JR (2003) J Power Sources 118:256
18. Taracon A, Norby T, Dezanneau G, Morata A, Peiro F, Morante JR (2004) Electrochem Solid-State Lett 7:A373
19. Marrero-Lopez D, Canales-Vazquez J, Ruiz-Morales JC, Rodriguez A, Irvine JTS, Nunez P (2005) Solid State Ion 176:1807
20. Wang JX, Wang XP, Liang FJ, Cheng ZJ, Fang QF (2006) Solid State Ion 177:1437
21. Bellino MG, Lamas DG, Walsoe de Reca NE (2006) Adv Funct Mater 16:107
22. Marrero-Lopez D, Ruiz-Morales JC, Nunez P, Abrantes JCC, Frade JR (2004) J Solid State Chem 177:2378